

# FARCLUSS: Fuzzy Adaptive Rebalancing and Contrastive Uncertainty Learning for Semi-Supervised Semantic Segmentation

Ebenezer Tarubinga<sup>a</sup>, Jenifer Kalafatovich<sup>a</sup>, Seong-Whan Lee<sup>a,\*</sup>

<sup>a</sup>*Department of Artificial Intelligence, Korea University, Seoul, Korea*

---

## Abstract

Semi-supervised semantic segmentation (SSSS) faces persistent challenges in effectively leveraging unlabeled data, such as ineffective utilization of pseudo-labels, exacerbation of class imbalance biases, and neglect of prediction uncertainty. Current approaches often discard uncertain regions through strict thresholding favouring dominant classes. To address these limitations, we introduce a holistic framework that transforms uncertainty into a learning asset through four principal components: (1) fuzzy pseudo-labeling, which preserves soft class distributions from top-K predictions to enrich supervision; (2) uncertainty-aware dynamic weighting, that modulate pixel-wise contributions via entropy-based reliability scores; (3) adaptive class rebalancing, which dynamically adjust losses to counteract long-tailed class distributions; and (4) lightweight contrastive regularization, that encourage compact and discriminative feature embeddings. Extensive experiments on benchmarks demonstrate that our method outperforms current state-of-the-art approaches, achieving significant improvements in the segmentation of under-represented classes and ambiguous regions.

**Keywords:** Semi-supervised learning, Semantic segmentation, Fuzzy pseudo-labeling, Contrastive learning, Uncertainty estimation

---

<sup>\*</sup>Corresponding author

*Email addresses:* [psychofict@korea.ac.kr](mailto:psychofict@korea.ac.kr) (Ebenezer Tarubinga), [jenifer@korea.ac.kr](mailto:jenifer@korea.ac.kr) (Jenifer Kalafatovich), [sw.lee@korea.ac.kr](mailto:sw.lee@korea.ac.kr) (Seong-Whan Lee)

## 1. Introduction

Semantic segmentation, defined as the process of assigning class labels to every pixel in an image, supports a range of critical applications, including autonomous driving and medical diagnostics. By facilitating pixel-level scene analysis, it supports systems that demand fine-grained environmental understanding [5]. Nonetheless, fully supervised segmentation techniques usually depend on extensive datasets with detailed annotations; this makes the method costly in fields like urban scene analysis or healthcare, where manual labelling is both expensive and time-consuming [1]. To mitigate this dependency on labeled data, semi-supervised semantic segmentation (SSSS) has emerged as a promising alternative. By leveraging a modest set of labeled images alongside abundant unlabeled data, SSSS frameworks strive to achieve performance comparable to fully supervised models while substantially reducing annotation requirements. Early work in this area centered on pseudo-labeling [12], wherein a teacher model generates approximate labels for unlabeled data that a student model subsequently learns from. Later research introduced consistency regularization [13], enforcing prediction invariance under various geometric or photometric transformations. Although these techniques have shown improvements, they remain constrained by three principal issues: suboptimal use of pseudo-labels, class imbalance in long-tailed datasets, and inadequate handling of prediction uncertainty.

A closer examination reveals three principal shortcomings in current SSSS methods: ineffective utilization of pseudo-labels, class imbalance biases, and excessive computational cost. Although recent approaches attempt to address these issues, they often lack comprehensive solutions. Firstly, most methods treat pseudo-label uncertainty as a liability. They discard low-confidence predictions via strict thresholding, overlooking subtle probabilistic relationships among plausible classes. For instance, a pixel at the boundary of 'sidewalk' and 'road' may carry near-equal probabilities for both classes, yet is often removed, forfeiting valuable supervisory signals. UniMatch [3] combines feature- and output-level consistency but relies on fixed confidence thresholds to generate hard pseudo-labels. As a result, ambiguous predictions are eliminated, especially near object boundaries or occluded regions, leading to loss of information.

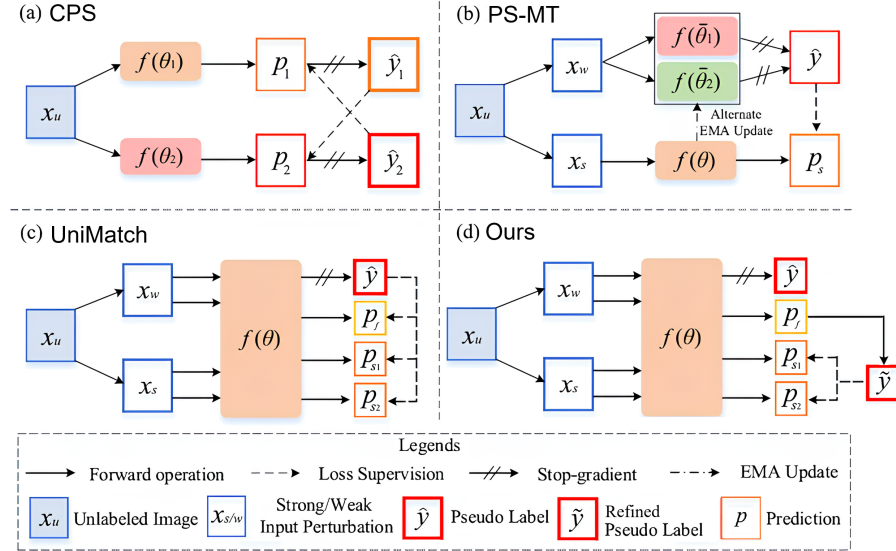


Figure 1: **Overview of consistency-regularization-based semi-supervised semantic segmentation (SSSS) frameworks** during training with unlabeled data.  $p_s$ ,  $p_f$ , and  $p_{sf}$  are predictions of strong input perturbation stream, feature perturbation stream, and strong input + feature perturbation stream.  $f(\theta)$  means exponential moving average (EMA) updated model.

Secondly, class imbalance remains inadequately addressed. Although some methods adjust global thresholds, they fail to rebalance losses based on per-batch class distributions, perpetuating bias toward majority classes. PS-MT [2] employs progressive self-training with momentum teachers and adaptive thresholds but lacks explicit mechanisms for class rebalancing. Consequently, dominant categories (e.g., "road" or "sky" in urban scenes) are over-represented in pseudo-labels.

Thirdly, contrastive learning frameworks often incur high computational cost due to extensive feature alignments, limiting scalability on large datasets. ReCo [4] improves feature discriminability using region-level contrastive learning, but its pairwise embedding comparisons introduce considerable overhead. Cross-pseudo supervision (CPS) [6] trains dual networks that supervise each other, yet applies uniform weighting to pseudo-labels, neglecting the need to treat uncertain regions differently.

In response, this work proposes a unified framework that systematically addresses

common challenges in semi-supervised segmentation, including pseudo-label noise, class imbalance, and computational overhead (Fig. 1). First, we introduce fuzzy pseudo-labeling, which derives soft label distributions from the top-K class probabilities at each pixel. By preserving uncertainty (unlike previous methods' strict thresholding), our method treats ambiguity as a constructive supervisory cue. This enables the model to learn from regions like unclear boundaries (e.g., pavement edges between "car" and "road") instead of discarding them.

Second, we implement uncertainty-aware dynamic weighting, assigning pixel-wise weights based on normalized entropy to modulate pseudo-label influence during training. This mechanism curbs the impact of noisy high-entropy regions (e.g., overlapping objects) while amplifying the contribution of confident predictions. This mechanism improves upon CPS by replacing uniform weighting with a more discriminative strategy [6].

Third, we propose adaptive class rebalancing to mitigate class imbalance by dynamically adjusting loss weights according to batch-level pseudo-label frequencies. This ensures under-represented categories like "traffic sign" or "tumor" receive adequate optimization focus without manual tuning.

Finally, we introduce lightweight contrastive regularization based on a prototype-centric design. By computing class-specific centroids from confidently labeled pixels, our approach promotes discriminative feature clustering while avoiding the computational burden of exhaustive pairwise comparisons as in ReCo [4].

While existing methods have tackled individual challenges such as ineffective pseudo-label utilization, class imbalance, and high computational cost, they often fall short of addressing these issues simultaneously within a unified and performant framework. The main contributions of this work are summarized as follows:

- **Fuzzy Pseudo-Labeling:** Constructs soft label distributions from top-K class probabilities, preserving ambiguity as a learning signal rather than discarding uncertain pixels.
- **Uncertainty-Aware Dynamic Weighting:** Modulates pixel-wise pseudo-label impact using normalized entropy, reducing noise from ambiguous regions and

enhancing learning from confident predictions.

- **Adaptive Rebalancing:** Dynamically scales losses based on pseudo-label frequencies per batch, improving learning for minority classes without manual heuristics.
- **Lightweight Contrastive Regularization** Prototype-based Contrastive learning via class centroids avoids costly pairwise operations while promoting feature compactness.

## 2. Related Works

### 2.1. Teacher-Student Frameworks and Pseudo-Label Refinement

Semi-supervised semantic segmentation (SSSS) has progressed remarkably through teacher-student paradigms, wherein models generate pseudo-labels from unlabeled data to guide training. Early work such as FixMatch [7] employed confidence thresholding to filter pseudo-labels, leading to high-confidence yet inaccurate predictions reinforced model errors (confirmation bias). Cross Pseudo Supervision (CPS) [6] mitigated this issue by training two networks jointly in a supervised manner using each other’s pseudo-labels, thereby diversifying the learning signal. PseudoSeg [8] enhanced reliability through augmented prediction fusion, while Directional Context-Aware Consistency (DC-Loss) [9] encouraged alignment of class-specific features in differing contexts. More recent approaches, including the Error Localization Network (ELN) [10] and UĂšPL [11], introduced modules to detect, filter, or reinterpret uncertain predictions as negative supervision. However, most of these methods still rely on strict thresholding, discarding ambiguous pixels and thereby limiting data usage. By contrast, our framework employs fuzzy pseudo-labeling to retain the top-K class probabilities for each pixel, preserving nuanced inter-class relationships and providing richer supervision even in low-confidence regions.

### 2.2. Uncertainty-Aware Confidence Calibration

Uncertainty estimation has become central to improving pseudo-label quality. For example, RePU [16] refined pseudo-labels using entropy-based uncertainty scores, and

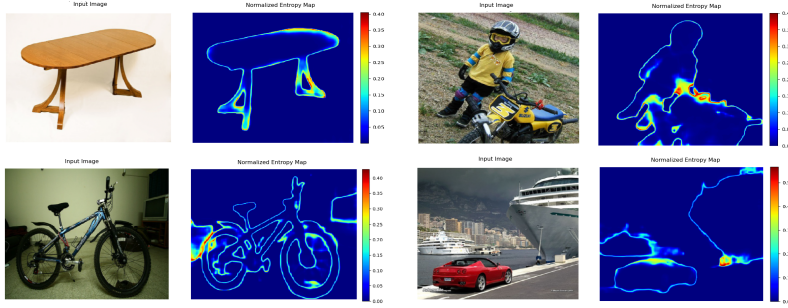


Figure 2: **Pixel-wise normalized entropy map from the teacher model on PASCAL VOC samples.** Brighter colors represent higher prediction uncertainty. Uncertainty is concentrated at object boundaries and cluttered background regions.

Bayesian Uncertainty Calibration [17] leveraged Monte Carlo dropout to identify unreliable predictions. Despite their effectiveness, these methods generally adopt uncertainty as a binary filter rather than as a learning signal. By contrast, our approach incorporates uncertainty-aware dynamic weighting, wherein normalized entropy modulates the contribution of each pseudo-label. High-entropy areas, such as boundaries or overlapping objects, are downweighted proportionately to their uncertainty, reducing noise while preserving partial supervisory information, a notable improvement over deterministic thresholding or uniform weighting.

### 2.3. Class Imbalance and Rare Class Enhancement

Class imbalance continues to pose significant challenges for SSSS, as pseudo-labels often exhibit a bias toward frequently occurring classes. DARS [18] aligned pseudo-label distributions with those from labeled data, and Adaptive Equalization Learning (AEL) [19] amplified underrepresented classes through adaptive loss weighting. Augmentation-based approaches, including Dynamic Cross-Set Copy-Paste (DCSCP) [20] and iMAS [21], artificially increased rare-class samples or dynamically adjusted supervision based on confidence. While these methods successfully address class imbalance, they typically rely on global class distributions, overlooking variations at the batch level. In contrast, our adaptive class rebalancing technique leverages per-batch pseudo-label frequencies to scale losses, ensuring that classes like traffic sign

in Cityscapes receive increased focus when they appear infrequently. Moreover, we employ a prototype-based contrastive regularization strategy, wherein class centroids derived from high-confidence pseudo-labels enhance intra-class compactness. Unlike ReCo [4], which entails computationally expensive pairwise comparisons, this prototype-based approach offers improved feature separability for minority classes with minimal overhead.

#### 2.4. Computational Efficiency and Lightweight Learning

Contemporary SSSS approaches frequently carry a high computational burden due to multi-model architectures or complex regularization. Cross-Consistency Training (CCT) [22] reduced this burden by training multiple decoder heads with a shared encoder, while UniMatch [3] illustrated that a single-network FixMatch [7] can achieve performance comparable to multi-model solutions. Multi-Granularity Distillation (MGD) [23] further improved efficiency via hierarchical knowledge distillation. Building on these principles, our framework avoids dual-network configurations like CPS [6] and auxiliary modules such as ELN [10]. Through single-pass fuzzy pseudo-labeling, entropy-based weighting, and prototype-based contrastive learning, we preserve scalability on large datasets without sacrificing segmentation accuracy.

### 3. Method

Our method integrates fuzzy pseudo-labeling, uncertainty-based dynamic weighting, adaptive class rebalancing, and efficient contrastive regularization to address inefficient pseudo-label utilization, class imbalance biases, and underutilization of uncertain predictions. An overview of our proposed method is shown in Fig. 3.

#### 3.1. Teacher-Student Architecture

We adopt a teacher-student framework inspired by classic mean-teacher approaches [24]. Let  $\mathcal{X}_l = \{(x_i^l, y_i^l)\}_{i=1}^{N_l}$  represent labeled training data, and  $\mathcal{X}_u = \{x_j^u\}_{j=1}^{N_u}$  be unlabeled training data. The student model, parameterized by  $\theta_s$ , is trained with labeled data on  $\mathcal{X}_l$  and with additional unlabeled data on  $\mathcal{X}_u$ . The teacher model, parameterized by  $\theta_t$ , provides pseudo-labels and is updated as an exponential moving

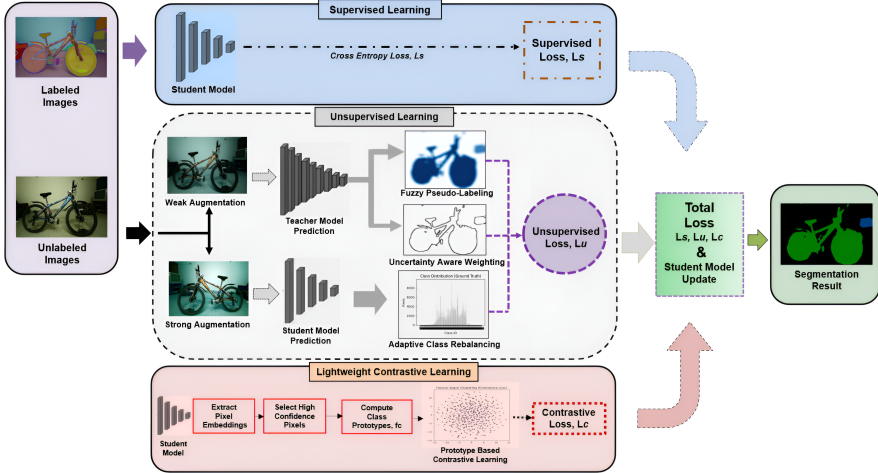


Figure 3: **Overview of the FARCLUSS Framework.** FARCLUSS employs a teacher-student framework where labeled data supervise the student directly, while unlabeled data undergo fuzzy pseudo-labeling and uncertainty-based weighting via the teacher. Adaptive class rebalancing and prototype-based contrastive learning further refine the total loss.

average (EMA) of the student’s weights. Specifically, after each training iteration  $k$ , weights are updated following:

$$\theta_t^{(k)} = \alpha \theta_t^{(k-1)} + (1 - \alpha) \theta_s^{(k)}, \quad (1)$$

where  $\alpha = 0.99$  is a momentum term that stabilizes the teacher’s evolution. This design helps smooth out noisy student updates.

### 3.2. Fuzzy Soft Pseudo-Labeling

Traditional pseudo-labeling strategies often rely on a single threshold to filter high-confidence predictions. While effective at removing noisy labels, such strict filtering can discard informative “uncertain” regions, thus underutilizing unlabeled data. To mitigate this, we propose *fuzzy soft pseudo-labeling* that retains more valuable information from the teacher’s predictive distribution.

#### 3.2.1. Fuzzy Pseudo-Label Generation

Given a teacher-generated probability map  $p^T \in \mathbb{R}^{C \times H \times W}$ , where  $C$  is the number of classes and  $(H, W)$  are spatial dimensions, we select the top- $K$  classes (by predicted

probability) at each pixel [47]:

$$\text{top}K(p_{:,h,w}^T) = \arg \text{sort}_{c \in \{1, \dots, C\}}(p_{c,h,w}^T)[:, :K]. \quad (2)$$

The fuzzy pseudo-label distribution  $p^{\text{fuzzy}}$  is then computed:

$$p_{c,h,w}^{\text{fuzzy}} = \frac{p_{c,h,w}^T \cdot \mathbf{1}_{c \in \text{top}K(p_{:,h,w}^T)}}{\sum_{c' \in \text{top}K(p_{:,h,w}^T)} p_{c',h,w}^T} \quad (3)$$

thus preserving a small set of plausible classes for each location instead of hard-assigning a single class or discarding uncertain pixels entirely. This fuzzy label distribution provides richer supervisory signals, particularly for borderline or potentially misclassified regions, improving the student's ability to learn from uncertain areas.

### 3.2.2. Unsupervised Loss with Fuzzy Labels

We incorporate the fuzzy label distribution into the unsupervised loss  $\mathcal{L}_u$  by measuring the KL divergence between the fuzzy pseudo-label  $p^{\text{fuzzy}}$  and the student's strongly-augmented output  $p^S$ :

$$\mathcal{L}_u = \frac{1}{N_{\text{valid}}} \sum_{h,w} M_{h,w} W_{h,w} \sum_{c=1}^C p_{c,h,w}^{\text{fuzzy}} \log\left(\frac{p_{c,h,w}^{\text{fuzzy}}}{p_{c,h,w}^S}\right). \quad (4)$$

Where,  $M_{h,w}$  is a binary mask indicating valid (non-ignored) pixels,  $W_{h,w}$  is a dynamic pixel-level weight tied to the teacher's prediction uncertainty and  $N_{\text{valid}}$  is the total number of valid pixels in a training batch.

By combining fuzzy soft labels and consistency regularization,  $\mathcal{L}_u$  enforces that the student's predictions on strongly-augmented images align with the teacher's more nuanced soft assignments on weakly-augmented inputs.

## 3.3. Uncertainty-Aware Dynamic Weighting

### 3.3.1. Per-Pixel Uncertainty Estimation

To address this noisy pseudo-labels, we modulate the contribution of each pixel to the unsupervised loss via a pixel-level weight  $W_{h,w}$  that inversely depends on normalized entropy. Fig 2 shows pixel-wise normalized entropy maps for several predictions from

the teacher model. Specifically, the normalized entropy  $H$  for the teacher’s prediction is:

$$H(p_{:,h,w}^T) = -\frac{1}{\log(C)} \sum_{c=1}^C p_{c,h,w}^T \log(p_{c,h,w}^T). \quad (5)$$

Since  $\log(C)$  is the maximum possible entropy (for a uniform distribution),  $H \in [0, 1]$  conveniently normalizes entropy across different numbers of classes.

### 3.3.2. Dynamic Weight Function

We then define the pixel-wise weight as:

$$W_{h,w} = 1 - H(p_{:,h,w}^T), \quad (6)$$

so that pixels with high uncertainty (close to 1) receive smaller weights, and pixels with low uncertainty (close to 0) have higher weights. This design preserves the benefits of fuzzy labeling while still suppressing contributions from extremely ambiguous teacher predictions.

## 3.4. Adaptive Class Rebalancing

### 3.4.1. Mitigating Class-Imbalance Bias

Semantic segmentation datasets often exhibit significant imbalance (e.g., “background” or common object classes can dominate less frequent classes). Under such skew, the model and pseudo-labels inevitably become biased toward majority classes, which can further degrade the quality of minority-class pseudo-labels.

To combat this, we adopt an *adaptive class rebalancing* scheme, computing per-class weights  $w_c$  based on the frequency of pseudo-labeled pixels in each training batch. Concretely, for each class  $c$ , let  $F_c$  denote the number of pseudo-labeled pixels. We then compute:

$$w_c = \frac{\text{median}(F)}{F_c + \epsilon}, \quad (7)$$

where  $\text{median}(F)$  is the median of  $\{F_c\}_{c=1}^C$  and  $\epsilon$  is a small constant (e.g.,  $10^{-6}$ ) to avoid division by zero.

### 3.5. Loss Reweighting

We integrate these class-level weights into the unsupervised loss as follows:

$$\mathcal{L}_u = \frac{1}{N_{\text{valid}}} \sum_{h,w} M_{h,w} W_{h,w} \sum_{c=1}^C w_c \cdot p_{c,h,w}^{\text{fuzzy}} \log\left(\frac{p_{c,h,w}^{\text{fuzzy}}}{p_{c,h,w}^S}\right). \quad (8)$$

By boosting contributions of minority-class pixels, the student receives stronger supervision signals for classes that otherwise might be overshadowed. This strategy is conceptually related to reweighting approaches seen in long-tailed classification but tailored here to the specifics of pixel-wise pseudo-label frequencies.

### 3.6. Efficient Contrastive Feature Regularization

#### 3.6.1. Prototype-Based Contrastive Framework

Beyond consistency-based training, modern semi-supervised methods often leverage contrastive objectives to better separate feature clusters [26, 27]. However, straightforward pixel-to-pixel contrast can be computationally expensive due to the sheer number of pixel embeddings per batch. We thus adopt a lightweight prototype-based approach that captures global class-specific representation while minimizing overhead.

For each class  $c$ , we collect all pixels  $i \in P_c$  whose fuzzy pseudo-labels are sufficiently confident (e.g., meeting a confidence threshold or having weight  $W_{h,w}$  above some small value). We compute the class prototype  $f_c$  as the average (mean) embedding of those pixels:

$$f_c = \frac{1}{|P_c|} \sum_{i \in P_c} f_i, \quad (9)$$

where  $f_i$  is the embedding (e.g., the output of a mid-level feature layer) for pixel  $i$ .

#### 3.6.2. Contrastive Loss

To encourage *intra-class compactness* and better semantic separation, we penalize the cosine distance between each pixel embedding  $f_i$  and its corresponding prototype  $f_c$ :

$$\mathcal{L}_{\text{contrastive}} = \frac{1}{C} \sum_{c=1}^C \frac{1}{|P_c|} \sum_{i \in P_c} (1 - \cos(f_i, f_c)). \quad (10)$$

This loss pulls pixel embeddings closer to their class centroid, effectively minimizing within-class variation. Because the prototypes are recomputed at each training step,

the model’s representations remain updated according to the most recent pseudo-label assignments.

### 3.7. Final Training Objective

#### 3.7.1. Combined Loss

Bringing all the pieces together, the overall loss is:

$$\mathcal{L}_{\text{total}} = \underbrace{\mathcal{L}_s}_{\text{supervised}} + \underbrace{\lambda_u \mathcal{L}_u}_{\text{unsupervised}} + \underbrace{\lambda_c \mathcal{L}_{\text{contrastive}}}_{\text{contrastive}}, \quad (11)$$

where:

$\mathcal{L}_s$  is the standard cross-entropy loss on labeled data  $\mathcal{X}_l$ :

$$\mathcal{L}_s = -\frac{1}{|\mathcal{X}_l|} \sum_{(x^l, y^l) \in \mathcal{X}_l} \sum_{h,w}^C y_{c,h,w}^l \log(p_{c,h,w}^s). \quad (12)$$

$\mathcal{L}_u$  is the KL-divergence-based unsupervised loss using fuzzy soft pseudo-labels and per-pixel weighting.

$\mathcal{L}_{\text{contrastive}}$  is the prototype-based contrastive loss.

$\lambda_u$  and  $\lambda_c$  are weighting factors, set to 0.5 and 0.1, respectively in our experiments.  $\lambda_u$  and  $\lambda_c$  balance the influence of the unsupervised and contrastive losses, respectively.

#### 3.7.2. Practical Considerations

*Batch Composition:* We typically sample both labeled and unlabeled examples within each mini-batch to ensure that every update uses both  $\mathcal{L}_s$  and  $\mathcal{L}_u$ .

*Memory and Efficiency:* Prototype-based contrastive regularization is kept efficient by reducing the dimensionality of the features (e.g., via a 128-D projection head) and limiting prototypes to only high-confidence pixels.

*Hyperparameter Tuning:* In practice,  $K$  for top- $K$  fuzzy pseudo-labels, the threshold for pixel “confidence” in the contrastive branch, and the weighting factors  $\lambda_u, \lambda_c$  can be further tuned per dataset for optimal performance.

---

**Algorithm 1** FARCLUSS pseudocode in PyTorch style

---

```
# f: encoder g + decoder h; f_ema: EMA teacher; aug_w/aug_s: perturbations
criterion_ce = nn.KLDivLoss(log_target=False, reduction="none")
criterion_con = nn.CosineSimilarity(dim=1)
m = 0.99 # EMA momentum # eq. 1
for x in loader_u:
    # generate weak/strong views
    xw = aug_w(x)
    xs1, xs2 = aug_s(xw), aug_s(xw)
    # teacher inference & fuzzy labels
    with torch.no_grad():
        pw = f_ema(xw)
        tk = pw.topk(K, 1).indices
        fuzzy = torch.zeros_like(pw).scatter_(1, tk, pw.gather(1, tk))
        fuzzy = fuzzy / fuzzy.sum(dim=1, keepdim=True) #eq. 2
        H = - (pw * pw.log()).sum(dim=1) / math.log(pw.shape[1])
        w_px = 1 - H # pixel/instance weight # eq. 6
    # student features & mask
    feat = g(torch.cat([xs1, xs2])) # B*2, C, H, W
    bs2, C, H, W = feat.shape
    m0 = torch.bernoulli(0.5 * torch.ones(bs2//2, C, device=feat.device))
    mask = torch.cat([m0, 1 - m0], 0).view(bs2, C, 1, 1)
    pred = h(feat * mask)
    # supervised loss on labeled batch
    x_l, y_l = next(iter(loader_s))
    loss_sup = nn.CrossEntropyLoss()(f(x_l).log_softmax(1), y_l)
    # adaptive class rebalancing loss
    lbl = fuzzy.argmax(1)
    cnt = lbl.bincount(minlength=pw.size(1)).float()
    w_cls = cnt.median() / (cnt + 1e-6) # eq. 7
    loss_u_map = criterion_ce(pred.log_softmax(1), fuzzy) # B*2 x C x H x W
    loss_u = (w_px.view(-1,1,1,1) * w_cls[lbl].view(-1,1,1,1) * loss_u_map).mean()
    # prototype contrastive loss
    sel = w_px > 0.5
    fs = feat[sel] # N_sel, C, H, W
    lb = lbl[sel]
    fs_vec = fs.mean((2,3)) # N_sel x C
    cnt_sel = lb.bincount(minlength=pw.size(1)).float()
    proto = torch.zeros(pw.size(1), C, device=feat.device)
    proto.index_add_(0, lb, fs_vec)
    proto = proto / (cnt_sel.unsqueeze(1) + 1e-6) # eq. 9
    loss_c = (1 - criterion_con(fs_vec, proto[lb])).mean() # eq. 10

    # update student & EMA
    loss = loss_sup + loss_u * loss_c * loss_c # eq. 11
    optimizer.zero_grad(); loss.backward(); optimizer.step()
    for pt, ps in zip(f_ema.parameters(), f.parameters()):
        pt.data.mul_(m).add_(ps.data, alpha=1-m)
```

---

## 4. Experiments

### 4.1. Implementation Details

Our model is implemented using PyTorch and trained on Pascal VOC and Cityscapes datasets following common semi-supervised segmentation setups [3]. We build upon a DeepLabV3+ baseline architecture with ResNet-50 and ResNet-101 backbones [14, 15] with dilation rates {6, 12, 18}, and adopt standard mean-teacher EMA updates [7]. Training is performed for 80 epochs with a batch size of 8 for Pascal and 240 epochs for Cityscapes. The initial learning rate is set to 0.001, following common practice.

We optimize the model with stochastic gradient descent (SGD) using a momentum factor of 0.9 and polynomial decay for the learning rate:

$$\eta(i) = \eta_0 \left(1 - \frac{i}{i_{\max}}\right)^{0.9},$$

where  $\eta_0$  is the initial learning rate,  $i$  is the current iteration, and  $i_{\max}$  is the total training iterations. Weight decay is set to  $10^{-4}$  for regularization. The mean-teacher momentum parameter  $\alpha$  is fixed at 0.99, updating the teacher model as an exponential moving average of the student model’s weights.

### 4.2. Datasets and Semi-Supervised Setups

#### 4.2.1. Pascal VOC (Classic & Blended)

We utilize the Pascal VOC 2012 dataset [40] comprising of 1,464 high-quality images with extensive labels for training and 1, 449 images for validation. We also perform experiments on the Blended PASCAL VOC2012 dataset which is augmented with the Segmentation Boundary Dataset (SBD) [48], enlarging the training pool to 10,582 images. We also apply the same settings as U2PL [29] for the Blended dataset evaluation. For semi-supervised learning experiments, we adopt the established practice of using fractions {1/16, 1/8, 1/4, 1/2} of the high-quality annotated images as labeled data, treating the remaining images as unlabeled. Evaluation is performed on the official validation set consisting of 1,449 images, and we report the performance in terms of mean Intersection-over-Union (mIoU).

#### 4.2.2. *Cityscapes*

The Cityscapes dataset [41] consists of 2,975 training images with fine-grained annotations and 500 validation images, featuring urban scenes labeled across 19 semantic classes. Despite its relatively smaller class space, Cityscapes offers high-resolution annotations (originally at 1024x2048 pixels), which include detailed labels for small and thin objects such as traffic lights. Model performance is evaluated by calculating the mIoU metric on the provided 500-image validation set.

#### 4.2.3. *Data Augmentation*

Following common practice in semi-supervised segmentation [22, 19], we apply weak augmentation (e.g., random scaling, random horizontal flipping) for teacher inference and strong augmentation (e.g., random crops, color jitter, stronger geometric transformations) for student training. Weakly-augmented images yield more stable teacher predictions, while strongly-augmented images regularize the student to learn robust features under varied conditions.

#### 4.2.4. *Hyperparameters*

*Pseudo-Labeling.* For fuzzy pseudo-labeling, we set  $K = 2$  for Pascal VOC and Cityscapes balancing complexity and memory constraints. A normalized entropy threshold of 0.7 is used to define high-uncertainty pixels, which are down-weighted via the uncertainty-based weight  $W_{h,w}$ .

*Class Rebalancing.* For each mini-batch, we estimate the class-frequency vector  $\{F_c\}_{c=1}^C$  over all pixels assigned to classes by the fuzzy pseudo-labels. The final weight  $w_c$  is computed with  $\epsilon = 10^{-6}$ .

*Contrastive Regularization.* For the prototype-based contrastive loss, we project intermediate feature maps into 128-D embeddings via a lightweight projection head. The hyperparameter  $\lambda_c$  in the final loss is set to 0.1, chosen based on preliminary experiments.

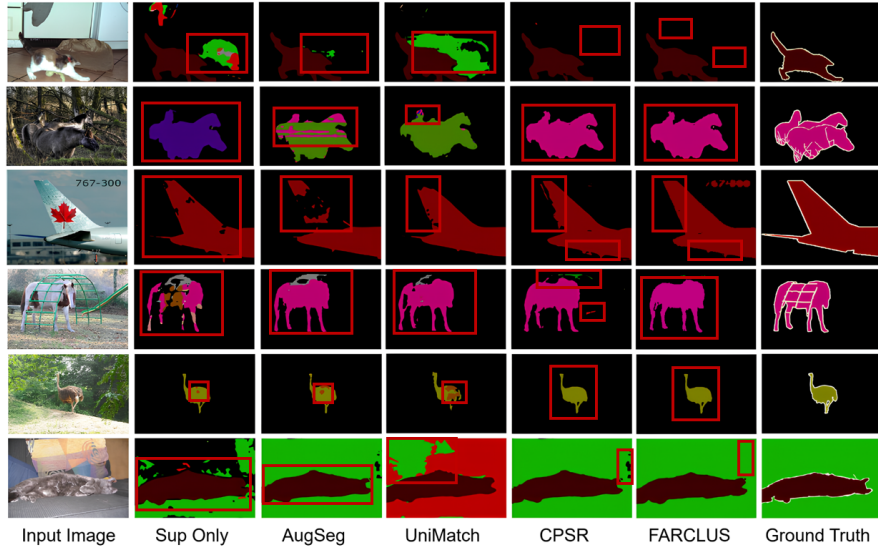


Figure 4: **Qualitative results of our method, FARCLUSS with other state-of-the-art methods on the PASCAL VOC 2012 dataset.** All methods are trained under the Full (1464) setting for validation. *Sup Only* refers to supervised baseline trained only on the corresponding proportion of labeled data. Red rectangles highlight regions where segmentation performance is improved.

#### 4.3. Comparisons with State-of-the-Art Methods

##### 4.3.1. Quantitative Analysis on Pascal VOC (Classic)

Table 1 shows the performance of our approach (FARCLUSS) compared to other SOTA methods on Pascal VOC across various labeled data ratios. We provide results for both ResNet-50 and ResNet-101 backbones, indicating the number of labeled examples in parentheses for each split. As shown, FARCLUSS consistently achieves competitive or superior mIoU across most labeled ratios, often ranking in the top three methods. Notably, our performance gains become more pronounced in lower supervision cases (e.g., 1/16 and 1/8 splits), where fuzzy pseudo-labeling and adaptive class rebalancing more effectively alleviate the scarcity of labeled samples.

##### 4.3.2. Quantitative Analysis on Pascal VOC (Blended)

Table 2 presents a comparison of FARCLUSS against state-of-the-art methods on the Pascal Blended Set using the mIoU (%) metric. All methods are trained with

Table 1: **Quantitative comparisons of state-of-the-art methods on the Pascal VOC classic** setting across different ratios (absolute number of labeled images is written in brackets). The highest values per split are in **red**, second highest in **green**, and third highest in **blue**.

Pascal SOTAs	Venue	ResNet-50					ResNet-101				Params
		1/16	1/8	1/4	1/2	Full	1/16	1/8	1/4	1/2	
		(92)	(183)	(366)	(732)	(1464)	(92)	(183)	(366)	(732)	
Supervised Only	-	44.00	52.30	61.70	66.70	-	45.1	55.3	64.8	69.7	59.5M
ST++ [28]	CVPR'22	72.60	74.40	75.40	-	79.10	65.2	71.0	74.6	77.3	59.5M
U <sup>2</sup> PL [29]	CVPR'22	63.30	65.50	71.60	73.80	75.10	68.0	69.2	73.7	76.2	59.5M
PS-MT [2]	CVPR'22	72.80	75.70	76.02	76.64	80.00	65.8	69.6	76.6	78.4	59.5M
GTA-Seg [30]	NeurIPS'22	-	-	-	-	-	70.0	73.2	75.6	78.4	59.5M
PCR [31]	NeurIPS'22	-	-	-	-	-	70.1	74.7	77.2	78.5	59.5M
AugSeg [32]	CVPR'23	64.22	72.17	76.17	77.40	78.82	71.1	75.5	78.8	80.3	59.5M
Diverse CoT [33]	ICCV'23	-	-	-	-	-	75.7	77.7	80.1	80.9	59.5M
ESL [34]	ICCV'23	61.74	69.50	72.63	74.69	77.11	71.0	74.0	78.1	79.5	59.5M
LogicDiag [35]	ICCV'23	-	-	-	-	-	73.3	76.7	77.9	79.4	59.5M
DAW [36]	NeurIPS'23	-	-	-	-	-	74.8	77.4	79.5	80.6	59.5M
UniMatch [3]	CVPR'23	71.90	72.48	75.96	77.09	78.70	75.2	77.2	78.6	79.9	59.5M
DDFP [37]	CVPR'24	-	-	-	-	-	75.0	78.0	79.5	81.2	59.5M
CorrMatch [38]	CVPR'24	-	-	-	-	-	76.4	78.5	79.4	80.6	59.5M
DUEB [43]	WACV'25	72.41	74.89	75.85	75.94	-	74.1	76.7	78.0	78.1	59.5M
CW-BASS [5]	IJCNN'25	72.80	75.81	76.20	77.15	-	-	-	-	-	59.5M
FARCLUSS	Ours	72.90	76.18	76.50	77.69	78.90	76.4	78.2	79.0	80.3	59.5M

the ‘aug’ setting, selecting labeled images from the VOC aug training set of 10,582 samples. Results are reported under two training resolutions: 321 and 513. The table distinguishes performance across different labeling ratios (1/16, 1/8, 1/4).

#### 4.3.3. Quantitative Analysis on Cityscapes

We further evaluate on Cityscapes, a more challenging urban-driving dataset with high-resolution images and multiple small classes. Table 3 provides comparisons to recent SOTA methods under partial-label settings.

Despite the greater complexity of Cityscapes (e.g., smaller objects, highly detailed street scenes), our method consistently ranks among the top methods at multiple supervision levels (1/8, 1/4, 1/2). Our fuzzy pseudo-labeling strategy provides fine-grained supervisory signals, beneficial for capturing small classes such as “rider” or “pole.” Similarly, adaptive class rebalancing helps counteract the long-tail distribution where cars, roads, and buildings dominate.

Table 2: **Quantitative comparisons of state-of-the-art methods on the Pascal Blended set** using different training resolutions (321 and 513). All methods are trained using the augmented training split (10,582 images). We evaluate both ResNet-50 and ResNet-101 backbones across three label ratios. The highest values per split are in **red**, second highest in **green**, and third highest in **blue**.

Pascal SOTAs	Train Size	Venue	ResNet-50			ResNet-101		
			1/16 (662)	1/8 (1323)	1/4 (2646)	1/16 (662)	1/8 (1323)	1/4 (2646)
SupOnly Baseline	321	-	61.2	67.3	70.8	65.6	70.4	72.8
CAC [9]	321	CVPR'21	70.1	72.4	74.0	72.4	74.6	76.3
ST++ [28]	321	CVPR'22	<b>72.6</b>	<b>74.4</b>	<b>75.4</b>	74.5	<b>76.3</b>	76.6
UniMatch [3]	321	CVPR'23	<b>74.5</b>	<b>75.8</b>	<b>76.1</b>	<b>76.5</b>	<b>77.0</b>	<b>77.2</b>
CorrMatch [38]	321	CVPR'24	-	-	-	<b>77.6</b>	<b>77.8</b>	<b>78.3</b>
FARCLUSS	321	Ours	<b>74.9</b>	<b>76.3</b>	<b>76.4</b>	<b>77.2</b>	<b>77.8</b>	<b>78.4</b>
SupOnly Baseline	513	-	62.4	68.2	72.3	67.5	71.1	74.2
CutMix-Seg [44]	513	BMVC'20	-	-	-	71.7	<b>75.5</b>	77.3
CCT [22]	513	CVPR'20	-	-	-	71.9	73.7	76.5
GCT [45]	513	ECCV'20	-	-	-	70.9	73.3	76.7
CPS [6]	513	CVPR'21	72.0	73.7	74.9	74.5	76.4	77.7
AEL [19]	513	NeurIPS'21	-	-	-	77.2	77.6	78.1
FST [46]	513	CVPR'22	-	-	-	73.9	76.1	78.1
ELN [10]	513	CVPR'22	-	-	-	-	75.1	76.6
U <sup>2</sup> PL [29]	513	CVPR'22	72.0	75.1	76.2	74.4	77.6	78.7
PS-MT [2]	513	CVPR'22	72.8	75.7	76.4	75.5	78.2	78.7
AugSeg [32]	513	CVPR'23	<b>74.6</b>	<b>76.0</b>	<b>77.2</b>	77.0	77.3	78.9
UniMatch [3]	513	CVPR'23	<b>75.8</b>	<b>76.9</b>	<b>76.8</b>	<b>78.1</b>	<b>78.4</b>	<b>79.2</b>
CorrMatch [38]	513	CVPR'24	-	-	-	<b>78.4</b>	<b>79.3</b>	<b>79.6</b>
FARCLUSS	513	Ours	<b>76.1</b>	<b>77.3</b>	<b>77.5</b>	<b>78.5</b>	<b>79.0</b>	<b>79.8</b>

#### 4.3.4. Quantitative Analysis on Computational Cost

Efficient utilization of unlabeled data in semi-supervised semantic segmentation critically influences performance, computational resources, and training stability. Comparative analysis with state-of-the-art methods show that FARCLUSS significantly reduces reliance on unlabeled data, matching the minimal requirements observed in recent approaches such as UniMatch [3] and CW-BASS [5] as shown in Table 4.

Earlier methods, including CPS [6], PS-MT [2], and ST++ [28], require extensive unlabeled datasets due to inherent architectural and training complexities. For example, CPS [6] employs dual networks generating mutual pseudo-labels, thus demanding extensive unlabeled data to sustain effective mutual supervision. For example, it processes 10.5k and 2.9k unlabeled images per epoch on Pascal VOC and Cityscapes, respectively. Its reliance on a fixed quantity of unlabeled data, irrespective of the labeled fraction,

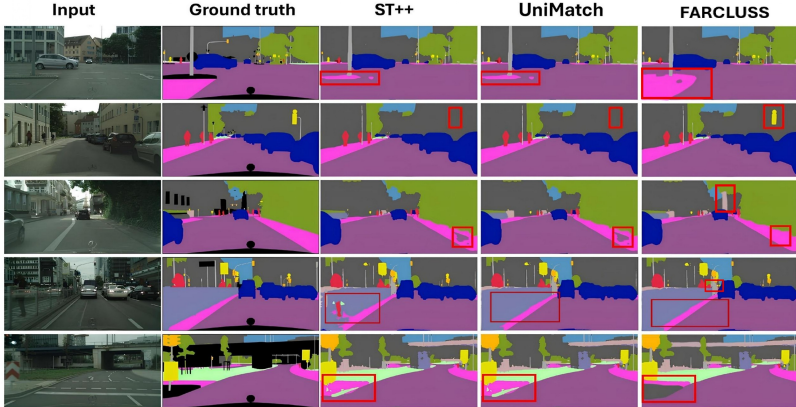


Figure 5: **Qualitative results of our method, FARCLUSS with other state-of-the-art methods on the Cityscapes dataset.** All methods are trained under the 1/8 (12%) setting for validation. Red rectangles highlight regions where segmentation performance is improved.

highlights the substantial data requirement for stable training outcomes.

Similarly, PS-MT [2] incorporates multiple perturbation methods (input, feature, and network-level) along with stringent confidence thresholds within three networks. Such complexities necessitate extensive unlabeled datasets to maintain robust consistency learning and reduce the impact of inaccurate pseudo-labels. It requires double or triple the unlabeled data and about 350-550 epochs on Cityscapes for model convergence. ST++ [28] uses self-training combined with selective retraining and robust data augmentations. These strategies substantially increase unlabeled data requirements (14.8k on Pascal, 4.1k on Cityscapes per epoch), especially under scenarios with low labeled data fractions, to ensure training stability.

UniMatch [3] adopts a streamlined weak-to-strong consistency framework using a shared student-teacher architecture. This reduces redundancy and enhances efficiency by utilizing consistency regularization without extensive pseudo-labeling, thereby effectively decreasing the required volume of unlabeled data. CW-BASS [5] introduces confidence-weighted losses and boundary-aware modules targeting confirmation bias and boundary ambiguities within a dual network using fewer augmentations. These enhancements allow the model to emphasize high-confidence regions, significantly lowering the necessity for large unlabeled datasets (up to 9.9k on Pascal, 2.7k on

Table 3: **Quantitative comparisons of state-of-the-art methods on the Cityscapes dataset** across different ratios (absolute number of labeled images is written in brackets). The highest values per split are in **red**, second highest in **green**, and third highest in **blue**.

Cityscapes SOTAs	Venue	ResNet-50				ResNet-101				Params
		1/16	1/8	1/4	1/2	1/16	1/8	1/4	1/2	
		(186)	(372)	(744)	(1488)	(186)	(372)	(744)	(1488)	
Supervised Only	-	63.34	68.73	74.14	76.62	66.3	72.8	75.0	78.0	59.5M
U <sup>2</sup> PL [29]	CVPR'22	69.00	73.00	76.30	78.60	74.9	76.5	78.5	79.1	59.5M
PS-MT [2]	CVPR'22	-	75.76	76.92	77.64	-	76.9	77.6	79.1	59.5M
GTA-Seg [30]	NeurIPS'22	-	-	-	-	69.4	72.0	76.1	-	59.5M
PCR [31]	NeurIPS'22	-	-	-	-	73.4	76.3	78.4	79.1	59.5M
AugSeg [32]	CVPR'23	73.70	76.40	78.70	79.30	75.2	77.8	79.6	80.4	59.5M
Diverse CoT [33]	ICCV'23	-	-	-	-	75.7	77.7	78.5	-	59.5M
ESL [34]	ICCV'23	71.07	76.25	77.58	78.92	75.1	77.2	78.9	80.5	59.5M
LogicDiag [35]	ICCV'23	-	-	-	-	76.8	78.9	80.2	81.0	59.5M
DAW [36]	NeurIPS'23	-	-	-	-	-	-	-	80.6	59.5M
UniMatch [3]	CVPR'23	75.03	76.77	77.49	78.60	76.6	77.9	79.2	79.5	59.5M
DDFP [37]	CVPR'24	-	-	-	-	77.1	78.2	79.9	80.8	59.5M
CorrMatch [38]	CVPR'24	-	-	-	-	77.3	78.4	79.4	80.4	59.5M
DUEB [43]	WACV'25	72.38	76.16	77.85	77.58	74.2	77.4	78.8	79.5	59.5M
CW-BASS [5]	IJCNN'25	75.00	77.20	78.43	-	-	-	-	-	59.5M
FARCLUSS	Ours	75.20	77.50	78.00	79.60	77.2	78.5	80.0	81.0	59.5M

Cityscapes).

FARCLUSS employs data-efficient techniques similar to UniMatch and CW-BASS, reducing reliance on large unlabeled datasets. The approach uses a shared student-teacher network with fuzzy pseudo-labeling to capture prediction uncertainty, while uncertainty-based weighting attenuates noise from erroneous pseudo-labels and stabilizes training. Adaptive class rebalancing addresses underrepresented classes, reducing the required dataset size for rare class representation and facilitating convergence without extensive unlabeled data-driven exploration. Consistent with efficient prior state-of-the-art methods, the model is trained for 80 epochs on Pascal and 240 epochs on Cityscapes. In this regard, our enhances data efficiency and reduces computational cost significantly.

Table 4: **Comparison on the Unlabeled data requirements to train all networks** of some state-of-the-art semi-supervised semantic segmentation methods on Pascal VOC 2012 and Cityscapes across multiple labeled data partitions. The table reports the number of unlabeled samples utilized during training per epoch.

Method	Networks	Pascal VOC 2012 (Classic)				Cityscapes			
		1/16	1/8	1/4	1/2	1/16	1/8	1/4	1/2
CPS [6]	2	10.5k	10.5k	10.5k	10.5k	2.9k	2.9k	2.9k	2.9k
ELN [10]	2	19.8k	18.5k	15.8k	10.5k	5.5k	5.2k	4.4k	2.9k
PS-MT [2]	3	19.8k	18.5k	15.8k	10.5k	5.5k	5.2k	4.4k	2.9k
ST++ [28]	4	14.8k	13.8k	11.9k	7.9k	4.1k	3.9k	3.3k	2.2k
UniMatch [3]	1	9.9k	9.2k	7.9k	5.2k	2.7k	2.6k	2.2k	1.4k
CW-BASS [5]	2	9.9k	9.2k	7.9k	5.2k	2.7k	2.6k	2.2k	1.4k
<b>FARCLUSS (Ours)</b>	<b>1</b>	<b>9.9k</b>	<b>9.2k</b>	<b>7.9k</b>	<b>5.2k</b>	<b>2.7k</b>	<b>2.6k</b>	<b>2.2k</b>	<b>1.4k</b>

#### 4.3.5. Qualitative Analysis

Figure 4 and 5 shows visual comparisons of segmentation outputs on Pascal VOC and Cityscapes. Our FARCLUSS model demonstrates clearer boundaries and improved recognition of minority classes (e.g., objects occupying a small fraction of the image). Fuzzy pseudo-labeling helps the student learn more stable decision boundaries around ambiguous regions, while the prototype-based contrastive learning better separates class embeddings.

#### 4.4. Ablation Study

To validate the contributions of each component in our framework, we conduct a comprehensive ablation study on the Pascal VOC (1/8 labeled data) and Cityscapes (1/8 labeled data) datasets using a ResNet-101 backbone. We systematically remove individual components while keeping others intact and analyze their impact on segmentation performance (mIoU). We evaluate the four key components of our method: Fuzzy Pseudo-Labeling ( $\mathcal{L}_f$ ), Uncertainty-Aware Weighting ( $W_{h,w}$ ), Adaptive Class Rebalancing ( $w_c$ ), and Contrastive Loss ( $\mathcal{L}_c$ ). The results are summarized in Table 5.

*Synergistic Effects.* The combined model exhibits super-additive improvements, reaching 78.2 mIoU on Pascal and 78.5 on Cityscapes (1/8 splits). Notably, fuzzy labeling and entropy weighting jointly allow learning from uncertain regions without degrading performance. Class rebalancing corrects label bias, and contrastive regularization

Table 5: **Ablation study on Pascal VOC 1/8 and Cityscapes 1/8 splits using ResNet-101**. Each row shows which components are active ( $\checkmark$ ). The mIoU reflects the performance of each configuration. Components:  $\mathcal{L}_f$  = fuzzy pseudo-labeling,  $W_{h,w}$  = uncertainty-based pixel-wise weighting,  $w_c$  = adaptive class rebalancing,  $\mathcal{L}_c$  = prototype contrastive loss.

Variant	$\mathcal{L}_f$	$W_{h,w}$	$w_c$	$\mathcal{L}_c$	Pascal 1/8	Cityscapes 1/8
Baseline ( $\mathcal{L}_s$ only)	$\times$	$\times$	$\times$	$\times$	55.3	72.8
w/o $\mathcal{L}_f$	$\times$	$\checkmark$	$\checkmark$	$\checkmark$	72.0	73.5
w/o $W_{h,w}$	$\checkmark$	$\times$	$\checkmark$	$\checkmark$	75.0	74.7
w/o $w_c$	$\checkmark$	$\checkmark$	$\times$	$\checkmark$	76.5	75.9
w/o $\mathcal{L}_c$	$\checkmark$	$\checkmark$	$\checkmark$	$\times$	77.5	78.1
<b>Full Method</b>	$\checkmark$	$\checkmark$	$\checkmark$	$\checkmark$	<b>78.2</b>	<b>78.5</b>

further refines representation quality. The interaction between these modules leads to improved generalization, greater training stability, and more balanced performance across the class spectrum.

#### 4.4.1. Component Analysis

*Fuzzy Pseudo-Labeling ( $\mathcal{L}_f$ ).* This module delivers the most substantial drop (-6.2 mIoU on Pascal), confirming its role in retaining informative supervision from ambiguous regions. By preserving top- $K$  class probabilities, fuzzy labels reduce confirmation bias and mitigate the overconfidence common in hard pseudo-labels. This mechanism aligns with entropy regularization and label smoothing, offering a continuous signal that better captures uncertainty, especially at object boundaries and for underrepresented classes.

*Uncertainty-Aware Weighting ( $W_{h,w}$ ).* Weighting pixel contributions using normalized entropy improves robustness by down-weighting noisy pseudo-labels, particularly in the early training stages. This acts as a soft curriculum, allowing the model to focus on high-confidence regions before incorporating noisier predictions. Removing this component results in a  $\sim$ 3.5 mIoU drop, indicating its importance in suppressing confirmation errors and ensuring stability.

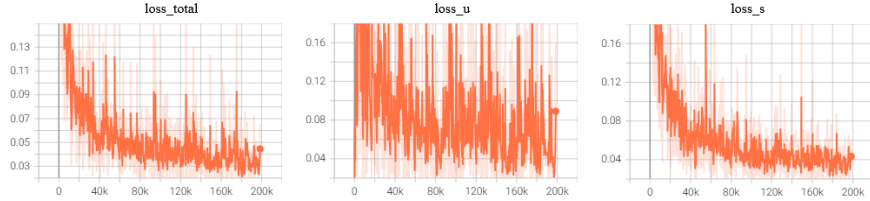


Figure 6: **Training trajectories of the total loss  $\mathcal{L}_{\text{total}}$  alongside its supervised component,  $\mathcal{L}_s$  and unsupervised component,  $\mathcal{L}_u$  over 200 k iterations on Pascal VOC with a 1/16 labelled split.**

*Adaptive Class Rebalancing ( $w_c$ ).* This component addresses the skewed distribution of pseudo-labels by adjusting loss contributions per class. It reduces performance, causing a 2.6 mIoU degradation in Cityscapes. The approach is theoretically supported by long-tail learning literature and empirically validated by prior methods such as DARS [18].

*Contrastive Loss ( $L_c$ ).* Though its isolated effect is more modest (0.5–0.7 mIoU), the contrastive loss enhances feature discriminability through intra-class compactness and inter-class separation. Our lightweight, prototype-based implementation avoids the computational cost of pairwise sampling and proves especially effective in disambiguating semantically similar regions.

#### 4.5. Loss-Convergence Dynamics

*Total Loss.* Figure 6 shows a monotonic descent from  $\approx 0.14$  to  $\approx 0.03$ . Because  $\lambda_c \ll \lambda_u$ , curvature is dominated by  $\mathcal{L}_s + \lambda_u \mathcal{L}_u$ ; spikes map directly to bursts in  $\mathcal{L}_u$ . The trend confirms stable optimisation and a negligible but beneficial contrastive term, consistent with findings in regional contrastive learning [4].

*Supervised Loss  $\mathcal{L}_s$ .* A rapid fall within the first  $4 \times 10^4$  updates reflects quick memorisation of the small labelled subset. The plateau near 0.04 indicates saturation once boundary-level errors dominate; labelled pixels contribute only 1/16 of batch gradients, limiting further reduction. Low variance follows from fixed one-hot labels and absence of entropy weighting.

*Unsupervised Loss  $\mathcal{L}_u$ .* An initial value  $> 0.16$  arises from wide-support pseudo-labels produced by an immature EMA teacher. High variance persists because pixel weights  $W_{h,w} = 1 - H(p_T)$  and class weights  $w_c$  are recomputed each iteration, a behaviour similarly reported in U<sup>2</sup>PL [29]. Downward drift to  $\approx 0.06$  evidences teacher refinement and entropy reduction; late-phase spikes coincide with adaptive boosting of minority classes, matching the goals of class rebalancing modules.

*Consistency with Prior Work.* Fuzzy pseudo-labelling preserves gradient signal in ambiguous regions, avoiding the loss collapse typical of hard-threshold methods such as FixMatch [7] or CPS [6]. Entropy weighting keeps variance bounded; regional contrastive regularisation supplies compact feature clusters with marginal numerical load. Observed dynamics replicate these effects, verifying correct implementation of FARCLUSS under extreme label scarcity.

#### 4.6. Further Quantitative Analysis on PASCAL VOC 2012 Classes’ Results

Table 6 quantitatively compares our proposed FARCLUSS method with supervised baseline, CPCL [49], and DUEB [43] approaches using the ResNet-50 backbone on specific PASCAL VOC 2012 dataset classes. Our approach demonstrates clear superiority, achieving the highest average mIoU scores across all data fractions (1/2, 1/4, 1/8, and 1/16), specifically attaining 77.69

In the Animal category (Bird, Cat, Cow, Dog, Horse, Sheep), FARCLUSS consistently outperforms competitors, reaching an impressive mIoU of 88.25% at 50% labeled data, surpassing the supervised baseline by 3.80%, CPCL by 1.62%, and DUEB by 1.17%. Similar trends are observed at lower labeling ratios, underscoring the effectiveness of our fuzzy pseudo-labeling and uncertainty-aware weighting mechanisms in accurately capturing animal class features.

The Vehicle category further highlights the robustness of FARCLUSS, attaining mIoUs of 79.86%, 80.17%, 80.02%, and 78.93% across several labeled partitions, consistently surpassing the supervised baseline and other SOTA methods. The improvements illustrate the method’s capability to mitigate common issues related to semantic confusion prevalent in vehicle segmentation.

Table 6: **Quantitative results on PASCAL VOC 2012 per class categories** of our method, FARCLUSS, and the Supervised Baseline, CPCL [49] & DUEB [43] methods using ResNet-50. Categories: **Animal** (Bird, Cat, Cow, Dog, Horse, Sheep), **Vehicle** (Aeroplane, Bicycle, Boat, Bus, Car, Motorbike, Train), **Indoor** (Bottle, Chair, Dining Table, Potted Plant, Sofa, Monitor), **Person**, and **Background**.

Methods	Avg mIoU				Animal				Vehicle			
	1/2	1/4	1/8	1/16	1/2	1/4	1/8	1/16	1/2	1/4	1/8	1/16
Supervised	74.05	71.66	67.16	62.00	84.45	78.98	73.47	67.65	76.90	74.31	71.94	67.88
CPCL [49]	75.30	74.58	73.74	71.66	86.63	85.39	84.24	82.73	77.23	76.62	76.53	76.24
DUEB [43]	75.94	75.85	74.89	72.41	87.08	86.69	85.47	84.66	78.25	78.60	78.75	77.09
<b>FARCLUSS (Ours)</b>	<b>77.69</b>	<b>76.50</b>	<b>76.18</b>	<b>72.90</b>	<b>88.25</b>	<b>87.89</b>	<b>86.50</b>	<b>85.73</b>	<b>79.86</b>	<b>80.17</b>	<b>80.02</b>	<b>78.93</b>
Methods	Indoor				Person				Background			
	1/2	1/4	1/8	1/16	1/2	1/4	1/8	1/16	1/2	1/4	1/8	1/16
Supervised	55.76	55.91	48.66	41.56	81.95	82.05	81.98	79.99	93.57	93.23	92.28	91.63
CPCL [49]	57.11	56.69	54.91	49.70	84.23	83.65	84.36	83.57	94.12	93.70	93.60	93.02
DUEB [43]	57.46	57.13	54.91	49.60	85.61	85.48	85.20	84.09	94.17	94.22	94.14	93.32
<b>FARCLUSS (Ours)</b>	<b>58.00</b>	<b>57.42</b>	<b>55.05</b>	<b>50.00</b>	<b>85.80</b>	<b>85.67</b>	<b>85.29</b>	<b>84.63</b>	<b>95.60</b>	<b>94.30</b>	<b>94.48</b>	<b>93.59</b>

Within the challenging Indoor class, FARCLUSS achieves improved mIoU performance compared to DUEB, the closest competitor. These incremental yet consistent improvements reflect the impact of adaptive class rebalancing and lightweight contrastive regularization in addressing feature ambiguities inherent in indoor object segmentation.

The Person category, traditionally stable across methods due to clearer semantic boundaries, still benefits notably from our method’s refined uncertainty treatment. FARCLUSS obtains marginally higher performances compared to DUEB’s performance, validating our holistic uncertainty transformation strategy.

Finally, FARCLUSS exhibits marked effectiveness in distinguishing Background, achieving top mIoU scores (95.60% to 93.59%) across all labeling ratios, reflecting its robust capacity for precise background segmentation and reduced false positives through uncertainty-aware dynamics.

Collectively, these results demonstrate the specific class gains of our FARCLUSS

framework, affirming its potential as a novel benchmark in semi-supervised semantic segmentation tasks, especially in scenarios characterized by limited annotations and class imbalance.

## 5. Conclusion

In this work, we introduced FARCLUSS, a unified framework designed to address critical limitations in semi-supervised semantic segmentation, including ineffective pseudo-labeling, class imbalance, and computational inefficiency. By integrating fuzzy pseudo-labeling, uncertainty-aware dynamic weighting, adaptive class rebalancing, and lightweight contrastive regularization, FARCLUSS enables a more informative and balanced learning. Extensive experiments on benchmark datasets confirm the superiority of our approach across multiple supervision regimes, especially for ambiguous and minority-class regions. FARCLUSS sets a new direction for uncertainty-guided, resource-efficient learning in semantic segmentation scenarios.

## References

- [1] T.-H. Vu, H. Jain, M. Bucher, M. Cord, and P. PĂlrez, “ADVENT: Adversarial Entropy Minimization for Domain Adaptation in Semantic Segmentation,” in *CVPR*, pp. 2517–2526, 2019.
- [2] Y. Liu *et al.*, “Perturbed and strict mean teachers for semi-supervised semantic segmentation,” in *CVPR*, pp. 4258–4267, 2022.
- [3] L. Yang *et al.*, “Revisiting Weak-to-Strong Consistency in Semi-Supervised Semantic Segmentation,” in *CVPR*, 2023.
- [4] G. Shin, W. Xie, and S. Albanie, “Reco: Retrieve and co-segment for zero-shot transfer,” *NeurIPS*, vol. 35, pp. 33754–33767, 2022.
- [5] E. Tarubinga, J. Kalafatovich and Seong-Whan Lee “CW-BASS: Confidence-Weighted Boundary-Aware Learning for Semi-Supervised Semantic Segmentation,” *arXiv preprint arXiv:2502.15152*, 2025.

- [6] X. Chen *et al.*, “Semisupervised semantic segmentation with cross pseudo supervision,” in *CVPR*, pp. 2613–2622, 2021.
- [7] K. Sohn *et al.*, “Fixmatch: Simplifying semi-supervised learning with consistency and confidence,” in *NeurIPS*, 2020.
- [8] Y. Zou *et al.*, “Pseudoseg: Designing pseudo labels for semantic segmentation,” *arXiv preprint arXiv:2010.09713*, 2020.
- [9] X. Lai *et al.*, “Semi-supervised semantic segmentation with directional context-aware consistency,” in *CVPR*, pp. 1205–1214, 2021.
- [10] D. Kwon and S. Kwak, “Semi-supervised semantic segmentation with error localization network,” in *CVPR*, pp. 9957–9967, 2022.
- [11] Y. Wang *et al.*, “Semi-supervised semantic segmentation using unreliable pseudo-labels,” in *CVPR*, pp. 4248–4257, 2022.
- [12] D. H. Lee, “Pseudo-Label: The Simple and Efficient Semi-Supervised Learning Method for Deep Neural Networks,” in *ICML Workshop on Challenges in Representation Learning*, pp. 896–901, 2013.
- [13] S. Laine and T. Aila, “Temporal ensembling for semi-supervised learning,” *arXiv preprint arXiv:1610.02242*, 2016.
- [14] K. He *et al.*, “Deep residual learning for image recognition,” in *CVPR*, pp. 770–778, 2016.
- [15] J. Deng *et al.*, “Imagenet: A large-scale hierarchical image database,” in *CVPR*, pp. 248–255, 2009.
- [16] Y. Zheng *et al.*, “RepUNet: A fast image semantic segmentation model based on convolutional reparameterization of ship satellite images,” in *CACRE*, pp. 461–465, IEEE, 2021.
- [17] Y. Cui *et al.*, “Bayesian Nested Neural Networks for Uncertainty Calibration and Adaptive Compression,” in *CVPR*, pp. 2392–2401, 2021.

- [18] Y. H. Cho *et al.*, “DARS: Data Augmentation using Refined Segmentation on Computer Vision Tasks,” in *ICTC*, pp. 348–350, IEEE, 2021.
- [19] H. Hu *et al.*, “Semi-supervised semantic segmentation via adaptive equalization learning,” *NeurIPS*, vol. 34, pp. 22106–22118, 2021.
- [20] J. Fan *et al.*, “UCC: Uncertainty Guided Cross-Head Co-Training for Semi-Supervised Semantic Segmentation,” in *CVPR*, pp. 9947–9956, 2022.
- [21] Z. Zhao *et al.*, “Instance-Specific and Model-Adaptive Supervision for Semi-Supervised Semantic Segmentation,” in *CVPR*, pp. 23705–23714, 2023.
- [22] Y. Ouali, C. Hudelot, and M. Tami, “Semi-Supervised Semantic Segmentation with Cross-Consistency Training,” in *CVPR*, pp. 12674–12684, 2020.
- [23] J. Qin *et al.*, “Multi-Granularity Distillation Scheme Towards Lightweight Semi-Supervised Semantic Segmentation,” in *ECCV*, pp. 481–498, Springer, 2022.
- [24] A. Tarvainen and H. Valpola, “Mean teachers are better role models: Weight-averaged consistency targets improve semi-supervised deep learning results,” in *NeurIPS*, 2017.
- [25] L.-C. Chen *et al.*, “Deeplab: Semantic image segmentation with deep convolutional nets, atrous convolution, and fully connected crfs,” *TPAMI*, vol. 40, no. 4, pp. 834–848, 2017.
- [26] T. Chen *et al.*, “A simple framework for contrastive learning of visual representations,” in *ICML*, 2020.
- [27] T. Zhou *et al.*, “C3-SemiSeg: Contrastive Semi-supervised Segmentation via Cross-set Learning and Dynamic Class-Balancing,” in *ICCV*, 2021.
- [28] J. Yang *et al.*, “ST++: Make self-training work better for semi-supervised semantic segmentation,” in *CVPR*, 2022.
- [29] Y. Wang *et al.*, “Semi-supervised semantic segmentation using unreliable pseudo-labels,” in *CVPR*, 2022.

- [30] X. Chen *et al.*, “Semi-supervised semantic segmentation with generalized task-aware consistency,” in *NeurIPS*, 2022.
- [31] T. Zhou *et al.*, “Semi-supervised semantic segmentation with pixel contrastive consistency,” in *NeurIPS*, 2022.
- [32] Y. Zhang *et al.*, “AugSeg: A simple data augmentation method for semi-supervised semantic segmentation,” in *CVPR*, 2023.
- [33] Y. Li *et al.*, “Diverse co-training for semi-supervised semantic segmentation,” in *ICCV*, 2023.
- [34] X. Chen *et al.*, “Semi-supervised semantic segmentation with entropy-based sample learning,” in *ICCV*, 2023.
- [35] T. Zhou *et al.*, “Semi-supervised semantic segmentation with logical diagnosis,” in *ICCV*, 2023.
- [36] Y. Li *et al.*, “Semi-supervised semantic segmentation with dual adaptive weighting,” in *NeurIPS*, 2023.
- [37] X. Chen *et al.*, “Semi-supervised semantic segmentation with dynamic dual feature propagation,” in *CVPR*, 2024.
- [38] T. Zhou *et al.*, “Semi-supervised semantic segmentation with correspondence matching,” in *CVPR*, 2024.
- [39] Y. Zhang *et al.*, “UniMatch: Unified semi-supervised learning for classification and segmentation,” in *CVPR*, 2023.
- [40] M. Everingham, S. A. Eslami, L. Van Gool, C. K. Williams, J. Winn, and A. Zisserman, “The Pascal Visual Object Classes Challenge: A Retrospective,” *International Journal of Computer Vision (IJCV)*, vol. 111, no. 1, pp. 98–136, 2015.
- [41] M. Cordts, M. Omran, S. Ramos, T. Rehfeld, M. Enzweiler, R. Benenson, U. Franke, S. Roth, and B. Schiele, “The Cityscapes Dataset for Semantic Urban Scene Understanding,” in *Proceedings of the IEEE Conference on Computer Vision and Pattern Recognition (CVPR)*, 2016, pp. 3213–3223.

- [42] T.-Y. Lin, M. Maire, S. Belongie, J. Hays, P. Perona, D. Ramanan, P. Dollár, and C. L. Zitnick, “Microsoft COCO: Common Objects in Context,” in *European Conference on Computer Vision (ECCV)*, 2014, pp. 740–755.
- [43] Smita Thakur, Rini and Vinod K. Kurmi, “Uncertainty and Energy based Loss Guided Semi-Supervised Semantic Segmentation,” *arXiv e-prints*, arXiv:2501, 2025.
- [44] G. French, S. Laine, T. Aila, M. Mackiewicz, and G. Finlayson, “Semi-supervised semantic segmentation needs strong, varied perturbations,” *arXiv preprint arXiv:1906.01916*, 2019.
- [45] Z. Xia, Y. Liu, Y. Wei, and Y. Yang, “Guided collaborative training for pixel-wise semi-supervised learning,” *arXiv preprint arXiv:2008.05258*, 2020.
- [46] Y. Du, Y. Shen, H. Wang, J. Fei, W. Li, L. Wu, R. Zhao, Z. Fu, and Q. Liu, “Learning from future: A novel self-training framework for semantic segmentation,” in *Advances in Neural Information Processing Systems*, vol. 35, 2022.
- [47] P. Qiao, Z. Wei, Y. Wang, Z. Wang, G. Song, F. Xu, X. Ji, C. Liu, and J. Chen, “Fuzzy positive learning for semi-supervised semantic segmentation,” in *Proc. IEEE/CVF Conf. Comput. Vis. Pattern Recognit.*, 2023, pp. 15465–15474
- [48] B. Hariharan, P. Arbeláez, L. Bourdev, S. Maji, and J. Malik, “Semantic contours from inverse detectors,” in *Proceedings of the 2011 International Conference on Computer Vision*, IEEE, 2011, pp. 991–998.
- [49] S. Fan, F. Zhu, Z. Feng, Y. Lv, M. Song, and F. Wang, “Conservative-progressive collaborative learning for semi-supervised semantic segmentation,” *IEEE Transactions on Image Processing*, vol. 32, pp. 6183–6194, 2023.